Automated EEG source imaging

A retrospective, blinded clinical validation study

Baroumand, Amir G.; van Mierlo, Pieter; Strobbe, Gregor; Pinborg, Lars H.; Fabricius, Martin; Rubboli, Guido; Leffers, Anne Mette; Uldall, Peter; Jespersen, Bo; Brennum, Jannick; Henriksen, Otto Mølby; Beniczky, Sándor

Published in:
Clinical Neurophysiology

DOI:
10.1016/j.clinph.2018.09.015

Publication date:
2018

Document version
Publisher's PDF, also known as Version of record

Clinical Neurophysiology 129 (2018) 2403–2410

Contents lists available at ScienceDirect

Clinical Neurophysiology

journal homepage: www.elsevier.com/locate/clinph

Automated EEG source imaging: A retrospective, blinded clinical validation study

Amir G. Baroumand [a], Pieter van Mierlo [a], Gregor Strobbe [b], Lars H. Pinborg [c,d], Martin Fabricius [e], Guido Rubboli [f], Anne-Mette Leffers [g], Peter Uldall [h], Bo Jespersen [i], Jannick Brennum [i], Otto Mølby Henriksen [j], Sándor Beniczky [k,l,*]

[a] Medical Image and Signal Processing Group, Department of Electronics and Information Systems, Ghent University – imec, De Pintelaan 185, 9000 Ghent, Belgium
[b] Epilog, Vlasgaardstraat 52, 9000 Ghent, Belgium
[c] Department of Neurology, Copenhagen University Hospital Rigshospitalet, Blegdamsvej 9, 2100 Copenhagen, Denmark
[d] Neurobiology Research Unit, Copenhagen University Hospital Rigshospitalet, 9 Blegdamsvej, DK-2100 Copenhagen, Denmark
[e] Department of Clinical Neurophysiology, Copenhagen University Hospital Rigshospitalet, Blegdamsvej 9, 2100 Copenhagen, Denmark
[f] Department of Neurology, Danish Epilepsy Centre, Kolonivej 1, 4293 Dianalund, Denmark
[g] Department of Diagnostic Radiology, Hvidovre Hospital, Kettegaard Alle 30, 2650 Hvidovre, Denmark
[h] Department of Paediatrics, Child Neurology, Copenhagen University Hospital Rigshospitalet, Blegdamsvej 9, 2100 Copenhagen, Denmark
[i] Department of Neurosurgery, Copenhagen University Hospital Rigshospitalet, Blegdamsvej 9, 2100 Copenhagen, Denmark
[j] Department of Clinical Physiology, Nuclear Medicine and PET, Copenhagen University Hospital Rigshospitalet, Blegdamsvej 9, 2100 Copenhagen, Denmark
[k] Department of Clinical Neurophysiology, Danish Epilepsy Centre, Visby Allé 5, 4293 Dianalund, Denmark
[l] Department of Clinical Neurophysiology, Aarhus University Hospital, Noerrebrogade 44, 8000 Aarhus, Denmark

ARTICLE INFO

Article history:
Accepted 15 September 2018
Available online 24 September 2018

Keywords:
Automation
EEG
Epilepsy
Presurgical evaluation
Source imaging
Source localization

HIGHLIGHTS

- We evaluated the accuracy of automated EEG source imaging in presurgical evaluation.
- The fully automated method had an accuracy of 61% (95% CI: 45–76%).
- The semi-automated method had an accuracy of 78% (95% CI: 62–89%).

ABSTRACT

Objective: To evaluate the accuracy of automated EEG source imaging (ESI) in localizing epileptogenic zone.

Methods: Long-term EEG, recorded with the standard 25-electrode array of the IFCN, from 41 consecutive patients with focal epilepsy who underwent resective surgery, were analyzed blinded to the surgical outcome. The automated analysis comprised spike-detection, clustering and source imaging at the half-rising time and at the peak of each spike-cluster, using individual head-models with six tissue-layers and a distributed source model (sLORETA). The fully automated approach presented ESI of the cluster with the highest number of spikes, at the half-rising time. In addition, a physician involved in the presurgical evaluation of the patients, evaluated the automated ESI results (up to four clusters per patient) in clinical context and selected the dominant cluster and the analysis time-point (semi-automated approach). The reference standard was location of the resected area and outcome one year after operation.

Results: Accuracy was 61% (95% CI: 45–76%) for the fully automated approach and 78% (95% CI: 62–89%) for the semi-automated approach.

Conclusion: Automated ESI has an accuracy similar to previously reported neuroimaging methods.

Significance: Automated ESI will contribute to increased utilization of source imaging in the presurgical evaluation of patients with epilepsy.

* Corresponding author at: Danish Epilepsy Centre, Visby Allé 5, 4293 Dianalund, Denmark.
E-mail address: sbz@filadelfia.dk (S. Beniczky).

https://doi.org/10.1016/j.clinph.2018.09.015
1388-2457/

1. Introduction

Approximately 1/3 of patients with epilepsy are drug-resistant (Kwan and Brodie, 2000). In this patient group, epilepsy surgery of the presumed epileptogenic focus is currently the treatment option with highest efficacy (Dwivedi et al., 2017; Engel et al., 2012; Wiebe et al., 2001). However, accurate localization of the epileptic focus is often challenging. Since there is no single-modality that reliably can localize the area that needs to be resected in order to render the patient seizure-free (EZ, epileptogenic zone), the presurgical evaluation is based on a multimodal approach (Rosenow and Lüders, 2001). This comprises semiology, EEG (obtained during long-term video-EEG monitoring), magnetic resonance imaging (MRI), and in selected cases positron emission tomography (PET), single photon emission computed tomography (SPECT) and magnetoencephalography (MEG).

Using this approach, only half of the investigated patients can be operated and of them only 2/3 become seizure free (Miller and Hakimian, 2013; Thom et al., 2010). Thus, there is need for additional methods, using post-processing and signal analysis that help localizing the EZ. EEG source imaging (ESI) estimates the underlying brain activity from the measured EEG, using an electric conduction model built from the patient's MRI. The value of ESI in the presurgical evaluation to localize the EZ has already been shown in several studies (Assaf and Ebersole, 1997; Beniczky et al., 2016; Boon et al., 2002; Brodbeck et al., 2011; Ding et al., 2007; Ebersole, 2000; Habib et al., 2016; Koessler et al., 2010; Kovac et al., 2014; Lantz et al., 1999; Lascano et al., 2016; Lu et al., 2012; Mégevand et al., 2014; Pellegrino et al., 2016; Staljanssens et al., 2017a; Staljanssens et al., 2017b; Strobbe et al., 2016; van Mierlo et al., 2017; Wennberg et al., 2011; Wennberg and Cheyne, 2014; Yang et al., 2011). Methods based on high-density (HD) EEG recordings and using individual head models (derived from the patient́s own MRI) proved more accurate than low-density (LD) recordings and models using template head models (Brodbeck et al., 2011).

In spite of the published compelling evidence on the accuracy of ESI, its use has not gained wide acceptance in clinical practice. In a recently published study, the E-pilepsy consortium showed that only 36% (9/25) of the European centers included ESI into their presurgical workup (Mouthaan et al., 2016). This is mainly because ESI is considered time-consuming and it requires special expertise in signal analysis that is not available in all centers. HD-EEG is typically recorded only for a few hours, since it is less feasible for long-term monitoring (Nemtsas et al., 2017). To overcome these obstacles and to contribute to more widespread use of ESI in presurgical evaluation, we have recently developed a fully automated process for identification and subsequent source localization of IEDs from long-term low-density EEG recordings (van Mierlo et al., 2017). Since almost all patients included in the presurgical evaluation undergo long-term EEG monitoring, preferably recorded using the standard electrode array setup of the IFCN (Seeck et al., 2017), and MRI scanning, these datasets are widely available in the epilepsy centers worldwide.

In this study, we present a clinical validation study on 41 operated patients using the automated method to detect and localize IEDs. As reference standard, we used the location of the surgical resection and postoperative outcome. Our goal was to determine the localization accuracy at sub-lobar level of the automated ESI method. Although the analysis was done retrospectively, it was blinded to all data other than the EEG recordings. Furthermore, the analyzed dataset was from a different institution than the ones where the automated method was developed. We present our results according to the STARD criteria (Bossuyt et al., 2016).

2. Methods

2.1. Patients and recordings

De-identified EEG and MRI data, from consecutive patients were analyzed retrospectively. These data were recorded as part of the clinical workup of the patients. Inclusion criteria were: patients with (1) drug-resistant focal epilepsy, (2) admitted to the Epilepsy Monitoring Unit (EMU) as part of the presurgical evaluation, (3) who underwent resective surgery, and (4) with postoperative follow-up of at least one year. Exclusion criterion was the lack of MRI sequences necessary for constructing the individual head model (see below). Patients gave their informed consent prior to admission to the EMU.

EEG was recorded at the Danish Epilepsy Centre, using the standardized IFCN array of 25 electrodes, including six electrodes in the inferior temporal chain (F9/10, T9/10 and P9/10) in addition to the 19 electrodes of the 10–20 system (Seeck et al., 2017). Electrode impedance was kept below 5KΩ. EEG was recorded with a sampling frequency of 256 Hz, using the NicoletOne system. For each patient, the complete, available EEG recording was analyzed (i.e. we did not select or exclude any EEG data).

MRI examination was done at Department of Radiology, Hvidovre Hospital, 3 T Siemens scanner. T1-3D-MPR-sequence was used for constructing the individual head models.

2.2. The analysis pipeline

De-identified long-term EEG and MRI data were analyzed using Epilog PreOp (Epilog NV, Ghent, Belgium). The analysis consists of automated spike detection, clustering of single detected spikes based on their morphology, and finally ESI analysis of the detected spikes at two time points: the half-rising time and the peak of the averaged spike waveforms. The whole analysis was performed blinded to all other data (clinical and para-clinical data, information on surgery and outcome). Fig. 1 shows the analysis pipeline.

2.3. Automated spike detection

Automated spike detection was performed using the Persyst Spike Detector P13 (Persyst, San Diego, CA, USA). Detected events with a spike-probability lower than 0.5 were rejected. After band-pass filtering the spikes from 0.5 to 30 Hz, those that contained a bad channel (i.e. a channel with a standard deviation that exceeds five times the median standard deviation of all channels) were excluded. The signals were baseline- corrected in a period of 200–100 ms before the peak of the spike. Afterwards, the spikes were averaged for each detected clusters and clusters were merged if the scalp topography at the peak had a correlation higher than 0.9. Clusters with less than 15 single spikes were excluded from further analysis. Up to four spike-clusters, with the highest number of spikes were further analyzed. The spikes within each cluster were averaged to increase signal-to-noise ratio (Wennberg and Cheyne, 2014).

Previously published, large-scale studies showed that although patients with focal epilepsy may have several interictal spike-clusters, analysis of the dominant cluster accurately localized the EZ (Brodbeck et al., 2011). However, criteria for determining the dominant spike-cluster have not been defined until now. We used two different criteria to determine which spike-cluster was dominant: quantitative and qualitative criteria. The quantitative criterion assumed that the cluster with much higher number of spikes, compared to the other clusters was the dominant one. Thus,

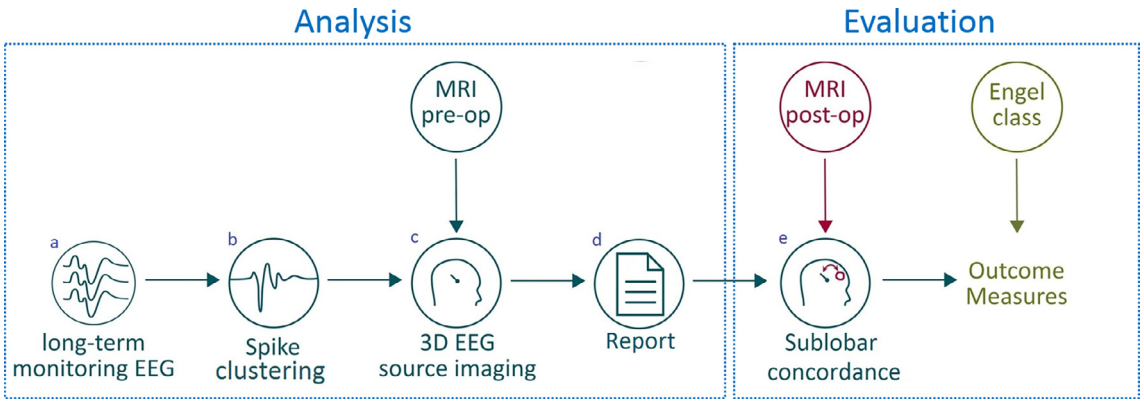

Fig. 1. The automated ESI (Epilog PreOp) pipeline: (a) recording long-term EEG signals, (b) detecting spikes using Persyst P13 spike detector, clustering them and averaging afterwards, (c) building patient-specific head model from the pre-operative MRI to perform ESI, (d) generating a report that summarizes the findings and (e) comparing the spike-clusters depicted in the report with the resection zone.

we considered a spike-cluster as quantitatively dominant if it contained at least twice as many spikes as all other clusters. When none of the identified clusters fulfilled this criterion, the patient was considered multifocal. The qualitative criteria aimed at reproducing the clinical reasoning, according to which each information is set into the broad clinical context, and weighed against all other data. Selection of the qualitatively dominant spike-cluster was done after completion of the automated analysis, by a physician in charge with the presurgical workup of the patients, and hence un-blinded to the clinical context.

2.4. Individual head model and inverse solution

For each patient, an individual head model with a $1 \times 1 \times 1$ mm resolution was constructed from the T1-weighted MR image. The head model consisted of six different tissues (scalp, skull, cerebrospinal fluid, grey matter, white matter and air) (Montes-Restrepo et al., 2016; Strobbe et al., 2016). To this end, each tissue probability map was estimated in the statistical parametric mapping software (SPM12). After smoothing, the maps were combined to form the head model. The skull thickness was set to a minimum of three voxels to ensure that no skull holes existed in the head models. The electrodes were placed on the head-model using the following procedure: (1) a 3D model was generated of the head model; (2) the nasion, inion and electrodes T7/T8, FT9/10, TP9/10 were marked on the 3D model; (3) the distances between the marked points over the surface of the head was used to place the other electrodes at inter-distances defined according to the 10–20 system; (4) visual inspection of the electrodes was done and if necessary individual electrodes were slightly moved to ensure correct placement of each electrode. (In some cases, we noticed that the position of electrodes P3 and P4 was slightly too lateral: because of the head curvature at that position the algorithm put them a bit too lateral. In these cases, we moved the electrodes slightly more central, but never more than 1 cm. For all other electrodes the positioning was kept as calculated). Afterwards, dipoles were placed in the gray matter with 3 mm spacing and the finite difference method was used to compute the leadfields that describe the relation between the current dipoles in the gray matter and the measured scalp EEG (Hallez et al., 2005; Strobbe et al., 2014; Vanrumste et al., 2001).

The source of each spike-cluster was localized at the half-rising time and at the peak of the spikes using sLORETA as inverse technique (Pascual-Marqui, 2002).

2.5. ESI reporting format

The Epilog ESI reports summarized the results of the automated analyses. Supplementary documents A and b show examples of ESI reports. The first page gives an overview of the detected spike-clusters together with the spike lateralization, spike timing and spike interval diagram. Then, for each cluster, the averaged and the ten most representative spikes are shown in both referential and bipolar montages. In the next pages, the EEG source localization at half-rising time and at peak are shown, both for the averaged spike and for 100 single spike-events that have most similar morphology compared to the averaged spike.

After completing the automated analyses, ESI reports were forwarded to the physician, who evaluated the automatically detected clusters, classifying them as epileptiform or non-epileptiform (artifacts), and then the qualitatively dominant clusters were identified as described above. In addition, depending on the clinical context, the physician could choose the ESI either at the half-rise time or at the peak.

This procedure resulted in two sets of results: those derived from the fully automated process (automated ESI, quantitative determination of the dominant cluster and analysis always at the half-rise time) and the results of the semi-automated approach (automated ESI, then selection of the dominant cluster and of the analysis time-point by the physician, in the clinical context). Non-dominant clusters and especially artifacts were more widely scattered than the spikes of the dominant clusters. This was taken into consideration when assessing the analysis reports. Three check boxes were included for each cluster (genuine spike, artefact, physiological) allowing the clinician to interpret and classify the clusters.

2.6. Reference standard

For evaluating the accuracy of the ESI, we used as reference standard the resected area and the outcome one year after surgery. All locations were determined at sub-lobar level (Beniczky et al., 2017). Patients with several clusters but without a dominant cluster were considered multifocal. Although distributed source models (such as sLORETA) result in spatially extended sources, similar to previous studies (Brodbeck et al., 2011) we determined the location of the sources at the maxima automatically indicated by the cross-hair in the source images. When this was inside the resected region, the localization was considered positive. Patients were considered seizure-free if they were Engel class I, at one year

post-operative follow-up. Results of the index test (ESI) were classified as follows: True Positive (TP): source within the resected area and seizure free outcome; False Positive (FP): source within the resected area and not seizure free outcome; True Negative (TN): source outside the resected area and not seizure free outcome; False Negative (FN): source outside the resected area and seizure free outcome. All patients with multifocal ESI and all patients without any spike-clusters were considered negative (i.e. discordant with the resected area).

2.7. Outcome measures

We calculated sensitivity, specificity, overall accuracy, positive predictive value (PPV), negative predictive value (NPV), and Odd's Ratio (OR) according to the conventional formulae:

$$sensitivity = \frac{TP}{TP + FN}$$

$$specificity = \frac{TN}{TN + FP}$$

$$overal\ \ accuracy = \frac{TP + TN}{TP + FP + TN + FN}$$

$$PPV = \frac{TP}{TP + FP}$$

$$NPV = \frac{TN}{TN + FN}$$

$$OR = \frac{sensitivity * specificity}{(1 - sensitivity) * (1 - specificity)}$$

95% confidence interval (95% CI) of a parameter was determined based on its standard error:

$$parameter\ \ standard\ \ error = \sqrt{\frac{parameter * (1 - parameter)}{sample\ \ size}}$$

$$95\%\ \ CI = \text{paremeter} \pm 1.96 * parameter\ \ standard\ \ error$$

where 1.96 expresses the normal distribution measure for 95% confidence interval. It could be used to measure intervals of sensitivity, specificity, accuracy, PPV and NPV (Griner et al., 1981; Mercaldo et al., 2007). However, calculation of 95% CI for OR was done according to the definitions described below (Bland, 2000):

$$standard\ \ error\ \ (\log(OR)) = \sqrt{\frac{1}{TP} + \frac{1}{TN} + \frac{1}{FP} + \frac{1}{FN}}$$

$$95\%\ \ CI\ \ (OR) = \exp(\log(\text{OR}) + 1.96 * standard\ \ error(\log(OR)))$$

3. Results

Out of 42 consecutive operated patients fulfilling the inclusion criteria, one patient was excluded due to the lack of a suitable MRI (Fig. 2). For this patient only CT imaging was available and not MRI. Data of 41 patients were analyzed (24 female; age: 12–55 years, median: 43 years, duration of analyzed EEG recording: 29 ± 3.9 h). Fourteen patients (34.1%) had normal MRI. Twenty-eight patients (68.3%) had temporal and 13 patients (31.7%) had extratemporal resections (six frontal, two parietal, two occipital, one mesial parieto-occipital, one insular and one operculo-insular resection). Twenty-five patients (61%) were seizure-free at one year follow-up.

In two patients, no interictal epileptiform discharges occurred during the LTM. Twelve patients had a single spike-cluster. In 22 patients, a dominant spike-cluster was identified using the quantitative criterion. In five patients with multiple clusters, none of them fulfilled the quantitative criterion for dominant cluster, and were classified as multifocal (thus discordant with the resection site).

Figs. 3 and 4 show the results of the ESI of a patient with temporal and respectively extratemporal focus. Supplementary document C details the results for all patients.

Table 1 summarizes the outcome measures. Using the fully automated method (quantitatively defined dominant cluster and

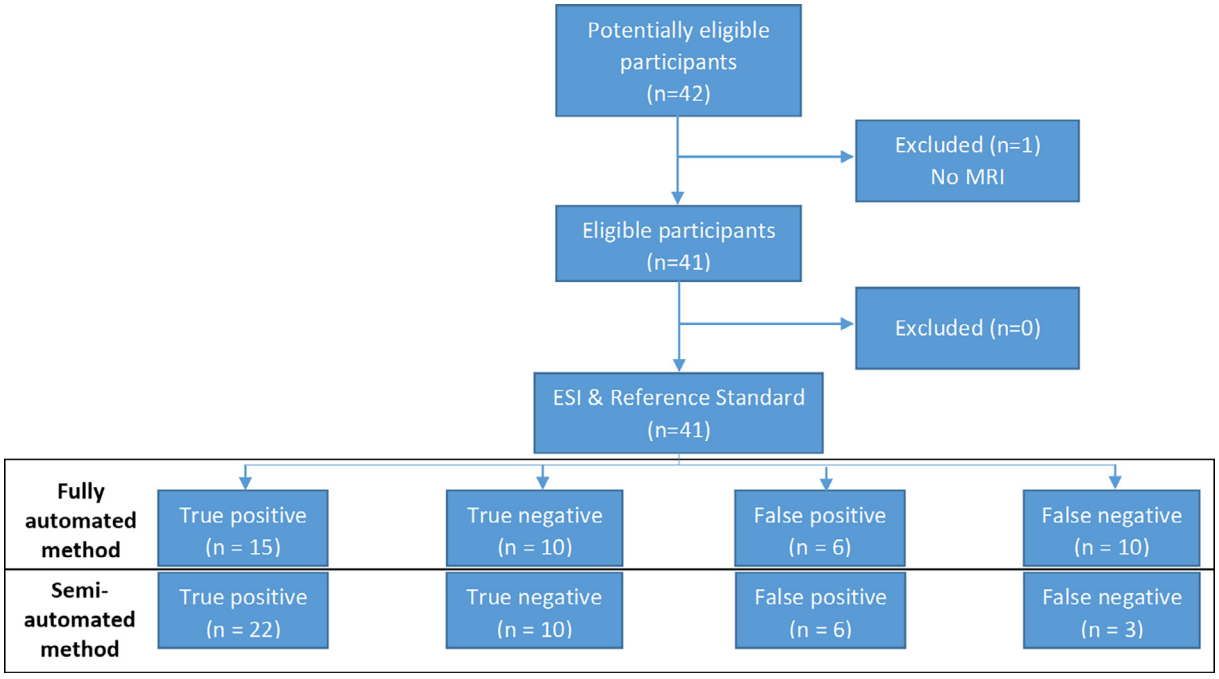

Fig. 2. Study flowchart. The fully automated method included: automated ESI of the spike-cluster with quantitatively identified cluster, at the half-rising time. The semi-automated method included: automated ESI and manual selection of the dominant cluster and analysis time-point (either half-rise or peak).

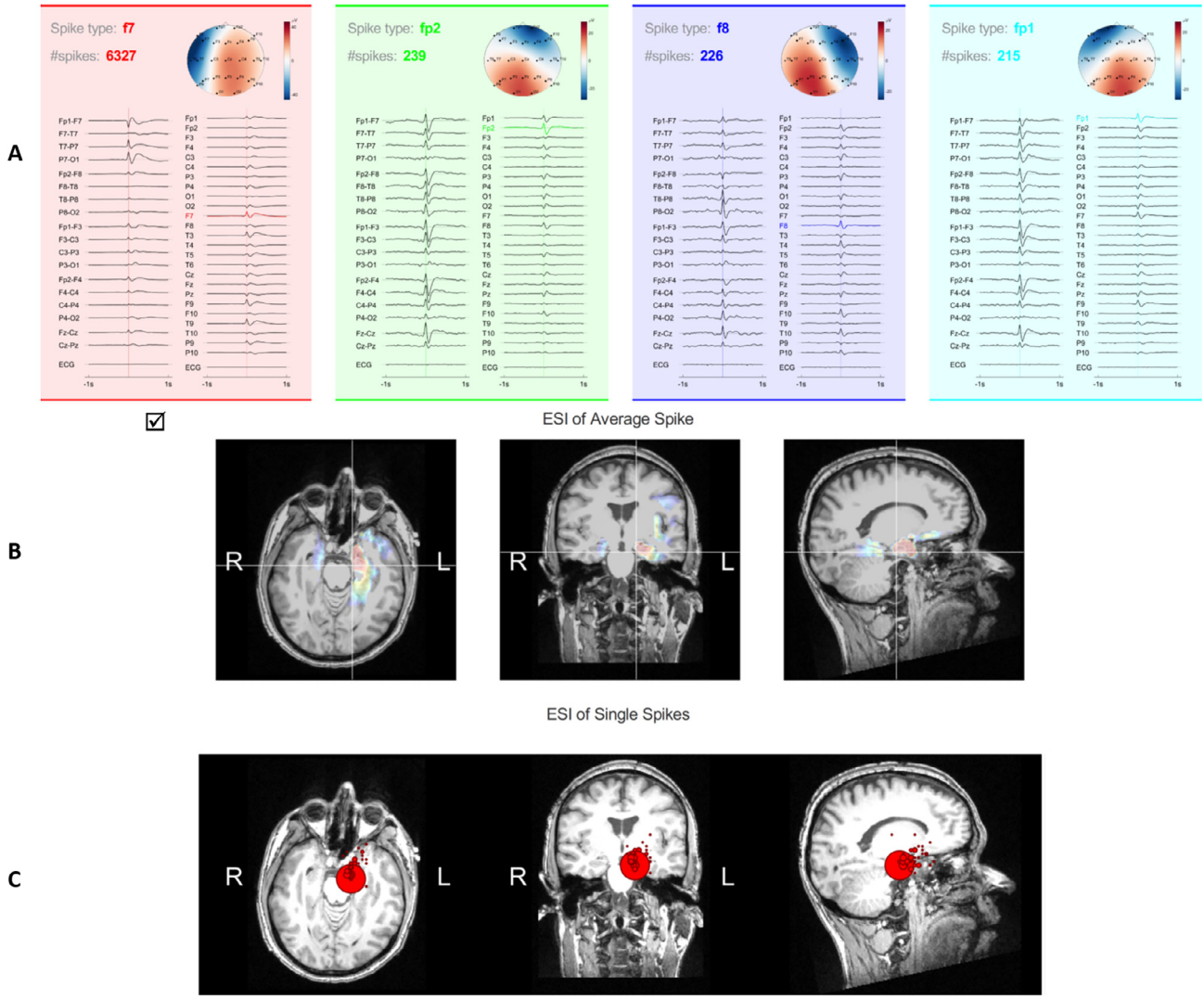

Fig. 3. ESI in a patient with temporal focus (patient #8). A: Four automatically detected spike-clusters. For each cluster, the following data are shown: name of the electrode closest to the peak-negativity, the number of spikes in the cluster, the averaged waveform (in longitudinal bipolar and referential montages) and the voltage map. Note that the first cluster is quantitatively dominant (it contains almost 10 times as many spikes as the other three clusters together). The same cluster was considered dominant by the physician who interpreted this in the clinical context (choice of the qualitative dominant spike is shown in the checkbox below the spike-cluster). B and C: Results of the automated ESI of the dominant spike-cluster, at the half-rise time of the averaged waveform (maximum localized at the crosshair) (B) and of the individual spikes in the cluster (C), respectively. Note that both the maximum of the averaged waveform, and the majority of the individual spikes (red circle) indicate a source in the left mesial temporal region, which was in concordance with the resection site. The pathological examination showed hippocampal sclerosis. The patient was seizure-free (Engel I) at the one-year postoperative follow-up. Supplementary document A shows the detailed analysis report of this patient. (For interpretation of the references to colour in this figure legend, the reader is referred to the web version of this article.)

analysis at half-rise time) gave an accuracy of 61%. In the semi-automated method, where physicians were allowed to choose the dominant cluster and the time-point of analysis (half-rise or peak) but still with automated detection and ESI, yielded an accuracy of 78%. The physician changed the choices of the fully automated method in seven patients (in one case the analysis time-point, in two cases the dominant cluster and in four cases both the time-point and the dominant cluster) (Supplementary document C). Although artifacts were often detected, they rarely were the quantitatively dominant clusters. In three of the cases where the users overruled the quantitatively dominant spike, this was due to artifacts.

4. Discussion

In this study, we validated the performance of automated long-term EEG analysis (van Mierlo et al., 2017) to localize the EZ. The algorithm detected interictal epileptiform discharges in the long-term EEG, clustered them and subsequently localized them using a realistic, patient-specific head model, built from the patient's MRI. The results were summarized in a concise report that was evaluated by a physician who was in charge with the presurgical evaluation of the patients. We evaluated two ways of implementing the automated ESI: a fully automated approach (quantitatively defined dominant cluster, analysis at half-rise) and a semi-automated approach, in which the physician was allowed to choose the dominant cluster and the analysis time-point (half-rise or peak). The fully automated approach yielded an accuracy of 61% (sensitivity: 60%, specificity, 63%). The semi-automated approach had better results (accuracy: 78%; sensitivity: 88%, specificity: 63%).

There are several important differences with respect to the previous study of automated ESI (van Mierlo et al., 2017). First of all, in this study, analysis was done completely blinded with respect to

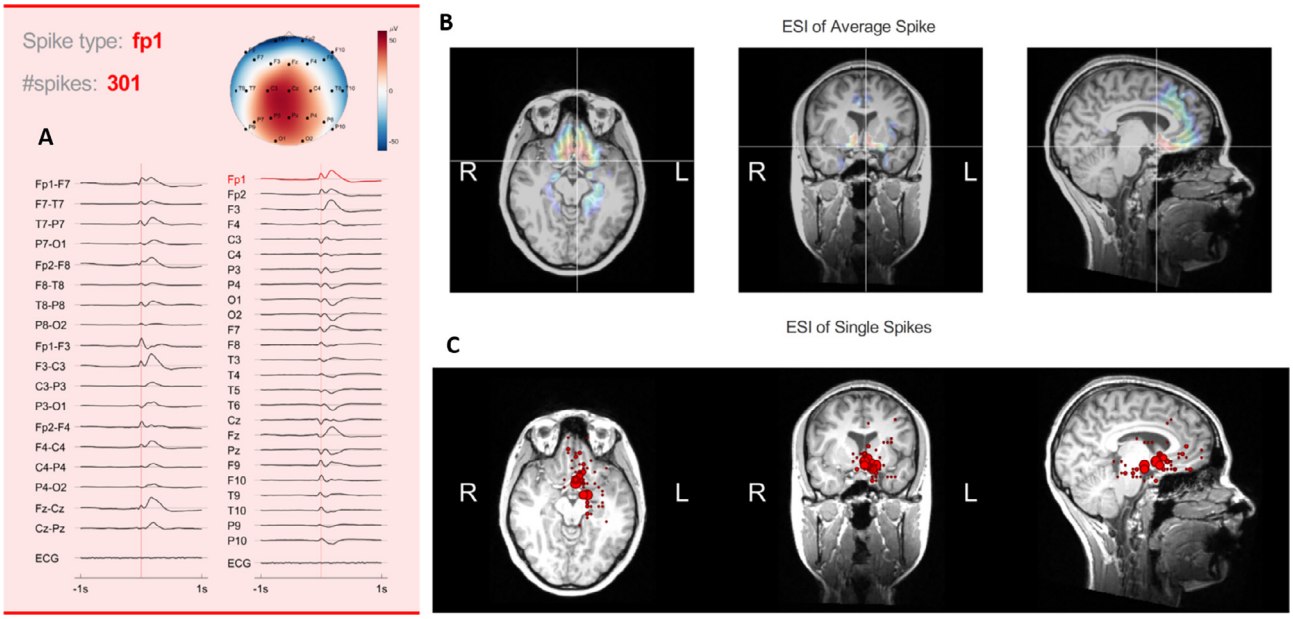

Fig. 4. ESI in a patient with frontal focus (patient #34). A: The automatically detected spike-cluster, specifying the name of the electrode closest to the peak-negativity, the number of spikes in the cluster, the averaged waveform (in longitudinal and referential montages) and the voltage map. In this patient, two clusters were automatically detected, but the second cluster was artifact (Supplementary document B). B and C: Results of the automated ESI, at the half-rise time of the averaged waveform (maximum localized at the crosshair) (B) and of the individual spikes in the cluster (C). Note that both the maximum of the averaged waveform, and the majority of the individual spikes (red circle) indicate a source in the left frontal basal-mesial region, which was in concordance with the resection site. The pathological examination showed focal cortical dysplasia (type IIb). The patient was seizure-free (Engel I) at the one-year postoperative follow-up. (For interpretation of the references to colour in this figure legend, the reader is referred to the web version of this article.)

Table 1
Accuracy measures of the automated ESI.

	Fully automated method	Semi-automated method
Accuracy (95% CI)	61% (45–76%)	78% (62–89%)
Sensitivity (95% CI)	60% (41–79%)	88% (75–100%)
Specificity (95% CI)	63% (39–85%)	63% (39–85%)
Positive predictive value (95% CI)	71% (52–91%)	79% (63–94%)
Negative predictive value (95% CI)	50% (28–72%)	77% (54–100%)
Odds ratio	2.5 (0.7–9.1)	12.2 (2.5–59)

patients' outcome. Only the anonymized, unmarked EEG recordings and T1-weighted MRI were included into the analysis dataset. The ESI-reports were made without any prior information and sent to the treating clinician, and then compared with the reference standard. Furthermore, the dataset used in this study was recorded in a different epilepsy center than those where the algorithm was developed, meaning that there is clear separation between the data used to develop the algorithm and the data used in this study to validate its performance. The algorithm was fixed upfront and was not tweaked based on the validation data. In this study, the concordance with the resection site (inside or outside the resected area) was used instead of the distance to the border of the resection to assess the clinical utility of the method.

An important finding of this study is that it identified two aspects that could not be optimally automated, and that needed intervention (decision) by the physician: the choice of the dominant cluster and the analysis time-point. This user-intervention was post-analysis, it was not time-consuming and did not need special expertise in signal analysis, since that part was automated. However, this step introduced subjective decisions and information outside ESI into the semi-automated analysis. This is a potential source of bias and we would like to point out that it is an important limitation of the semi-automated method.

In all large studies in literature, the EZ was estimated by localizing the dominant spike-cluster (Brodbeck et al., 2011; Lascano et al., 2016). However, the term "dominant cluster" was never precisely defined. We built the fully automated method on the assumption that the cluster with the highest number of spikes is the dominant one. Our results showed that this was not always the case.

In this study, we use both a quantitative and qualitative definition of the dominant cluster, demonstrating that interpretation of the ESI results based on the clinical context, improves its performance. This is in accordance with the clinical decision process in which data are weighed against all other available data. Moreover, since the frequency of spikes in different clusters can change significantly throughout the long-term monitoring (Scherg et al., 2012), the timing of the analyzed recording determines which cluster is quantitatively dominant: a cluster can contain many spikes one day, can only have few spikes the next day. In our study the mean duration of the EEG that was analyzed was 29 h. This ensures that a more general view of the occurrence of spikes was achieved compared to short recordings of 30 min to 1 h.

The other aspect that needs assessment by the physician is the time-point of the analysis. The half-rising time has previously been suggested as an ideal choice, because it is closer to the onset and the signal-to-noise ratio (SNR) is satisfactory in most clusters (Lantz et al., 2003). A problem with this strategy is that the spikes are averaged aligned to the peak time-point. Even within the same cluster, the morphology and duration of single spikes can vary. The further away from the peak the analysis is performed, the more variance (jitter) is introduced into the averaged signal (Fig. 5). This is consistent with a previous study that found source localization more reliable at the peak than at onset, in a sub-group of patients (Mălîia et al., 2016). Although the signal of the peak can be generated by brain areas to which the epileptic activity propagates from the EZ, peak has some advantages: the signal-to-noise ratio at the peak is higher than the one of the onset and half-rising, and, the

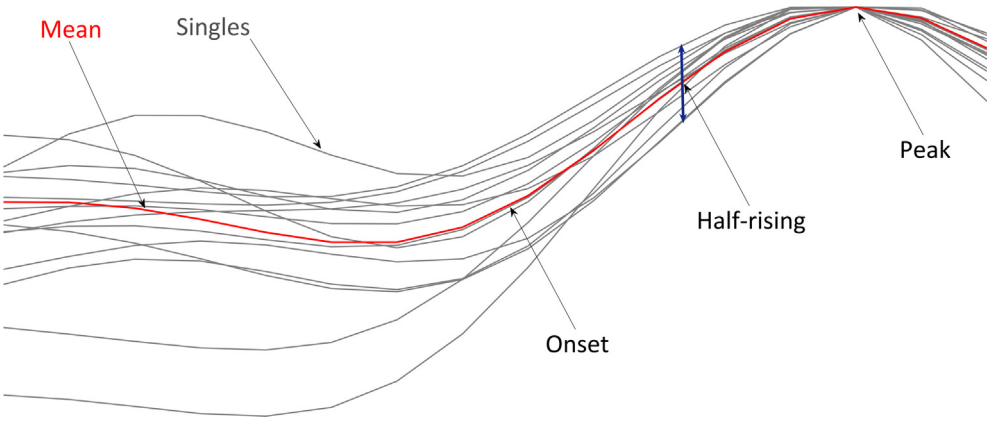

Fig. 5. Superposition of the single-spikes in a cluster of spikes. Note that the jitter (difference between the single-spikes) is larger at the half-rising time-point compared to peak.

jitter is lower, since spikes are averaged aligned to the peak. This explains why in five patients in this study, a better result was obtained at the peak of the spike compared to the half-rising time.

Because there is no reliable objective (automated) way to determine which cluster is the dominant one, and whether ESI is better at half-rise or at peak, optimally these decisions are taken by the physician, in the clinical context. This approach improves the performance of the automated ESI. Because the ESI reports include all necessary information for the clinicians, only a short time investment is necessary to make these choices. This removes the significant time-burden of the analysis process, and makes this approach feasible in a busy clinical setting.

Due to their architecture and the closed fields, spikes confined to amygdala and hippocampus do not generate signals of amplitude high enough to cross the scalp and these signals are not recorded by scalp electrodes, thus, these generators cannot be localized. This is an intrinsic limitation to any source imaging method. The maxima (cross-hair) of the mesial temporal sources we detected (like the one in Fig. 3) were in the nearby neocortical structures in the mesial part of the temporal lobe: the parahippocampal gyrus and the fusiform gyrus. Due to averaging of large numbers of spikes within each cluster, the signal-to-noise ratio is considerably improved, making possible localization of signals of lower amplitudes (like the middle third of the spike). This is in accordance with previously published large-scale studies that localized mesial temporal sources using distributed source models (Brodbeck et al., 2011).

The performance of EEG source imaging for localization of the EZ has previously been evaluated in several studies (Table 2). Brodbeck et al., 2011 indicated a sensitivity and specificity of 66% and 59% (n = 98) using low density EEG recordings, which increased to 84% and 88% (n = 52) using high density EEG. van Mierlo et al., 2017 analyzed low density ESI and they reported the values of 70% and 100% for sensitivity and specificity when peak of the first cluster was analyzed. By considering the first two clusters however, the sensitivity increased to 79% and specificity decreased to 75%. A recently published prospective study using the same electrode-array (IFCN 25 electrode array) found that ESI had an accuracy of 57–62%, which was in the same range as the conventional neuroimaging: MRI (55%), PET (33%) and SPECT (40%) (Sharma et al., 2018). This emphasizes the need for multimodal approach, since none of the methods achieves a sufficient accuracy on its own. Mégevand et al., 2014 and Lascano et al., 2016 used HD-ESI which lead to sensitivity and specificity of 80% and 59% (n = 32) or 88% and 47% (n = 58), respectively. However, working with HD EEG recording requires its specific setup, which is not broadly available. A potential bias in the HD-EEG is related to the patient-selection, since patients without spikes in the long-term monitoring, are typically not referred to the short duration (30–60 min) HD-EEG recordings. This might have led to an overestimation of its performance, since normal EEG recordings were not included into the evaluation of HD-EEG.

The performance of the ESI methods, including the automated methods described in this paper, are compatible (or even better) than the conventional neuroimaging methods (Supplementary document D). Nevertheless, each method delivers part of the complete picture. We cannot tell up front which investigation will be meaningful in which patient. Therefore, the inclusion of more techniques in the presurgical evaluation is beneficial for the localization of the EZ.

The added value of ESI could not be inferred from our retrospective dataset. Our study addressed the accuracy and not the clinical utility. A recently published systematic review and IFCN guideline on the utility of EEG in diagnosing and monitoring epilepsy (Tatum et al., 2018) concluded that in spite of the compelling published evidence for the accuracy of ESI, there is lack of evidence for its

Table 2
Performance of ESI for localization of EZ in some studies with the sample rates >20 patients.

Study	LD-ESI			HD-ESI		
	Sensitivity	Specificity	n	Sensitivity	Specificity	n
Mégevand et al. 2014	–	–	–	80%	59%	32
Brodbeck et al. 2011	66%	59%	98	84%	88%	52
Lascano et al. 2016	–	–	–	88%	47%	58
van Mierlo et al. 2017	70%	100%	32	–	–	–
Sharma et al. 2018	63%	47%	47			
Baroumand et al. 2018 (this study)	Fully automated: 60% Semi-automated: 88%	Fully automated: 63% Semi-automated: 63%	41	–	–	–

Abbreviations: LD = low-density, HD = high density, ESI = EEG source imaging.

clinical utility (i.e. diagnostic added value). Prospective studies, in which the multidisciplinary epilepsy surgery team makes first a preliminary decision blinded to the ESI data, and then modifies the decision based on ESI data are needed to elucidate the clinical utility of ESI.

The input data to our automated ESI (long-term EEG using $\geq$25 electrodes and T1-weighted MRI) are largely available in most centers doing presurgical evaluation, this method can be added to the multimodal work-up without additional time-burden. We hope that automating the analysis pipeline will contribute to increased utilization of ESI in the epilepsy centers.

Disclosure of conflicts of interest

Authors P.v.M. and G.S. are shareholders of Epilog NV. The remaining authors do not have conflicts of interests related to this work. We confirm that we have read the Journal's position on issues involved in ethical publication and affirm that this report is consistent with those guidelines.

Funding

This project received funding from the innovation program under the Marie Sklodowska-Curie grant agreement No. 660230.

Author statements

The corresponding author, Sándor Beniczky, has full access to all data and the right to publish such data. All authors participated in a meaningful way in the preparation of the manuscript.

Appendix A. Supplementary material

Supplementary data to this article can be found online at https://doi.org/10.1016/j.clinph.2018.09.015.

References

Assaf BA, Ebersole JS. Continuous source imaging of scalp ictal rhythms in temporal lobe epilepsy. Epilepsia 1997;38:1114–23.
Beniczky S, Rosenzweig I, Scherg M, Jordanov T, Lanfer B, Lantz G, et al. Ictal EEG source imaging in presurgical evaluation: high agreement between analysis methods. Seizure 2016;43:1–5.
Beniczky S, Aurlien H, Brøgger JC, Hirsch LJ, Schomer DL, Trinka E, et al. Standardized computer-based organized reporting of EEG: SCORE - Second version. Clin Neurophysiol 2017;128:2334–46.
Bland M. An introduction to medical statistics. 3rd ed. Oxford: Oxford University Press; 2000.
Boon P, D'Havé M, Vanrumste B, Van Hoey G, Vonck K, Van Walleghem P, et al. Ictal source localization in presurgical patients with refractory epilepsy. J Clin Neurophysiol 2002;19:461–8.
Bossuyt PM, Cohen JF, Gatsonis CA, Korevaar DA. STARD 2015: updated reporting guidelines for all diagnostic accuracy studies. Ann Transl Med 2016;4:85.
Brodbeck V, Spinelli L, Lascano AM, Wissmeier M, Vargas MI, Vulliemoz S, et al. Electroencephalographic source imaging: a prospective study of 152 operated epileptic patients. Brain 2011;134:2887–97.
Ding L, Worrell GA, Lagerlund TD, He B. Ictal source analysis: localization and imaging of causal interactions in humans. Neuroimage 2007;34:575–86.
Dwivedi R, Ramanujam B, Chandra PS, Sapra S, Gulati S, Kalaivani M, et al. Surgery for drug-resistant epilepsy in children. N Engl J Med 2017;377:1639–47.
Ebersole JS. Noninvasive localization of epileptogenic foci by EEG source modeling. Epilepsia 2000;41:S24–33.
Engel Jr J, McDermott MP, Wiebe S, Langfitt JT, Stern JM, Dewar S, et al. Early surgical therapy for drug-resistant temporal lobe epilepsy: a randomized trial. JAMA 2012;307:922–30.
Griner PF, Mayewski RJ, Mushlin AI, Greenland P. Selection and interpretation of diagnostic tests and procedures. Prin Appl Ann Intern Med 1981;94:555–600.
Habib MA, Ibrahim F, Mohktar MS, Kamaruzzaman SB, Rahmat K, Lim KS. Ictal EEG source imaging for presurgical evaluation of refractory focal epilepsy. World Neurosurg 2016;88:576–85.
Hallez H, Vanrumste B, Van Hese P, D'Asseler Y, Lemahieu I, Van de Walle R. A finite difference method with reciprocity used to incorporate anisotropy in electroencephalogram dipole source localization. Phys Med Biol 2005;50:3787–806.
Koessler L, Benar C, Maillard L, Badier JM, Vignal JP, Bartolomei F, et al. Source localization of ictal epileptic activity investigated by high resolution EEG and validated by SEEG. Neuroimage 2010;51:642–53.
Kwan P, Brodie MJ. Early identification of refractory epilepsy. N Engl J Med 2000;342:314–9.
Kovac S, Chaudhary UJ, Rodionov R, Mantoan L, Scott CA, Lemieux L, et al. Ictal EEG source imaging in frontal lobe epilepsy leads to improved lateralization compared with visual analysis. J Clin Neurophysiol 2014;31:10–20.
Lantz G, Michel CM, Seeck M, Blanke O, Landis T, Rosén I. Frequency domain EEG source localization of ictal epileptiform activity in patients with partial complex epilepsy of temporal lobe origin. J Clin Neurophysiol 1999;110:176–84.
Lantz G, Spinelli L, Seeck M, de Peralta Menendez RG, Sottas CC, Michel CM. Propagation of interictal epileptiform activity can lead to erroneous source localizations: a 128-channel EEG mapping study. J Clin Neurophysiol 2003;20:311–9.
Lascano AM, Perneger T, Vulliemoz S, Spinelli L, Garibotto V, Korff CM, et al. Yield of MRI, high-density electric source imaging (HD-ESI), SPECT and PET in epilepsy surgery candidates. Clin Neurophysiol 2016;127:150–5.
Lu Y, Yang L, Worrell GA, Brinkmann B, Nelson C, He B. Dynamic imaging of seizure activity in pediatric epilepsy patients. Clin Neurophysiol 2012;123:2122–9.
Mălîia MD, Meritam P, Scherg M, Fabricius M, Rubboli G, Mîndruță I, et al. Epileptiform discharge propagation: analyzing spikes from the onset to the peak. Clin Neurophysiol 2016;127:2127–33.
Mégevand P, Spinelli L, Genetti M, Brodbeck V, Momjian S, Schaller K, et al. Electric source imaging of interictal activity accurately localises the seizure onset zone. J Neurol Neurosurg Psychiatry 2014;85:38–43.
Mercaldo ND, Lau KF, Zhou XH. Confidence intervals for predictive values with an emphasis to case-control studies. Stat Med 2007;26:2170–83.
Miller JW, Hakimian S. Surgical treatment of epilepsy. Continuum 2013;19:730–42.
Montes-Restrepo V, Carrette E, Strobbe G, Gadeyne S, Vandenberghe S, Boon P, et al. The role of skull modeling in EEG source imaging for patients with refractory temporal lobe epilepsy. Brain Topogr 2016;29:572–89.
Mouthaan BE, Rados M, Barsi P, Boon P, Carmichael DW, Carrette E, et al. Current use of imaging and electromagnetic source localization procedures in epilepsy surgery centers across Europe. Epilepsia 2016;57:770–6.
Nemtsas P, Birot G, Pittau F, Michel CM, Schaller K, Vulliemoz S, et al. Source localization of ictal epileptic activity based on high-density scalp EEG data. Epilepsia 2017;58:1027–36.
Pascual-Marqui RD. Standardized low-resolution brain electromagnetic tomography (sLORETA): technical details. Methods Find Exp Clin Pharmacol 2002;24:5–12.
Pellegrino G, Hedrich T, Chowdhury R, Hall JA, Lina JM, Dubeau F, et al. Source localization of the seizure onset zone from ictal EEG/MEG data. Hum Brain Mapp 2016;37:2528–46.
Rosenow F, Lüders H. Presurgical evaluation of epilepsy. Brain 2001;124:1683–700.
Scherg M, Ille N, Weckesser D, Ebert A, Ostendorf A, Boppel T, et al. Fast evaluation of interictal spikes in long-term EEG by hyper-clustering. Epilepsia 2012;53:1196–204.
Sharma P, Scherg M, Pinborg LH, Fabricius M, Rubboli G, Pedersen B, et al. Ictal and interictal electric source imaging in pre-surgical evaluation: a prospective study. Eur J Neurol 2018. https://doi.org/10.1111/ene.13676.
Seeck M, Koessler L, Bast T, Leijten F, Michel C, Baumgartner C, et al. The standardized EEG electrode array of the IFCN. Clin Neurophysiol 2017;128:2070–7.
Staljanssens W, Strobbe G, Holen RV, Birot G, Gschwind M, Seeck M, et al. Seizure onset zone localization from ictal high-density EEG in refractory focal epilepsy. Brain Topogr 2017a;30:257–71.
Staljanssens W, Strobbe G, Van Holen R, Keereman V, Gadeyne S, et al. EEG source connectivity to localize the seizure onset zone in patients with drug resistant epilepsy. Neuroimage Clin 2017b;16:689–98.
Strobbe G, van Mierlo P, De Vos M, Mijović B, Hallez H, Van Huffel S, et al. Bayesian model selection of template forward models for EEG source reconstruction. NeuroImage 2014;93:11–22.
Strobbe G, Carrette E, López JD, MontesRestrepo V, Van Roost D, Meurs A, et al. Electrical source imaging of interictal spikes using multiple sparse volumetric priors for presurgical epileptogenic focus localization. Neuroimage Clin 2016;11:252–63.
Tatum WO, Rubboli G, Kaplan PW, Mirsatari SM, Radhakrishnan K, Gloss D, et al. Clinical utility of EEG in diagnosing and monitoring epilepsy in adults. Clin Neurophysiol. 2018;129:1056–82.
Thom M, Mathern GW, Cross JH, Bertram EH. Mesial temporal lobe epilepsy: How do we improve surgical outcome? Ann Neurol 2010;68:424–34.
van Mierlo P, Strobbe G, Keereman V, Birot G, Gadeyne S, Gschwind M, et al. Automated long-term EEG analysis to localize the epileptogenic zone. Epilepsia Open 2017;2:322–33.
Vanrumste B, Van Hoey G, Van de Walle R, D'Havé MR, Lemahieu IA, Boon PA. The validation of the finite difference method and reciprocity for solving the inverse problem in EEG dipole source analysis. Brain Topogr 2001;14:83–92.
Wennberg R, Valiante T, Cheyne D. EEG and MEG in mesial temporal lobe epilepsy: where do the spikes really come from? Clin Neurophysiol 2011;122:1295–313.
Wennberg R, Cheyne D. EEG source imaging of anterior temporal lobe spikes: validity and reliability. Clin Neurophysiol 2014;125:886–902.
Wiebe S, Blume WT, Girvin JP, Eliasziw M. A randomized, controlled trial of surgery for temporal-lobe epilepsy. N Engl J Med 2001;345:311–8.
Yang L, Wilke C, Brinkmann B, Worrell GA, He B. Dynamic imaging of ictal oscillations using non-invasive high-resolution EEG. Neuroimage 2011;56:1908–17.